NVU dynamics. II. Comparing to four other dynamics

Trond S. Ingebrigtsen, Søren Toxvaerd, Thomas B. Schrøder, and Jeppe C. Dyre[a)]
DNRF Centre "Glass and Time," IMFUFA, Department of Sciences, Roskilde University, Postbox 260, DK-4000 Roskilde, Denmark

(Received 28 March 2011; accepted 17 July 2011; published online 8 September 2011)

In the companion paper [T. S. Ingebrigtsen, S. Toxvaerd, O. J. Heilmann, T. B. Schrøder, and J. C. Dyre, "*NVU* dynamics. I. Geodesic motion on the constant-potential-energy hypersurface," J. Chem. Phys. (in press)] an algorithm was developed for tracing out a geodesic curve on the constant-potential-energy hypersurface. Here, simulations of NVU dynamics are compared to results for four other dynamics, both deterministic and stochastic. First, NVU dynamics is compared to the standard energy-conserving Newtonian NVE dynamics by simulations of the Kob-Andersen binary Lennard-Jones liquid, its WCA version (i.e., with cut-off's at the pair potential minima), and the Lennard-Jones Gaussian liquid. We find identical results for all quantities probed: radial distribution functions, incoherent intermediate scattering functions, and mean-square displacement as function of time. Arguments are presented for the equivalence of NVU and NVE dynamics in the thermodynamic limit; in particular, to leading order in $1/N$ these two dynamics give identical time-autocorrelation functions. In the final part of the paper, *NVU* dynamics is compared to Monte Carlo dynamics, to a diffusive dynamics of small-step random walks on the constant-potential-energy hypersurface, and to Nosé-Hoover NVT dynamics. If time is scaled for the two stochastic dynamics to make single-particle diffusion constants identical to that of NVE dynamics, the simulations show that all five dynamics are equivalent at low temperatures except at short times. © *2011 American Institute of Physics*. [doi:10.1063/1.3623586]

I. INTRODUCTION

In the companion paper (Paper I[1]), we developed a stable numerical algorithm for tracing out a geodesic curve on the constant-potential-energy hypersurface Ω of a system of N classical particles. If $U(\mathbf{r}_1, \ldots, \mathbf{r}_N)$ is the potential energy as a function of the particle coordinates, for a given value U_0 of the potential energy Ω is the $(3N-1)$-dimensional Riemannian differentiable manifold defined by (where $\mathbf{R} \equiv (\mathbf{r}_1, \ldots, \mathbf{r}_N)$ is the position in the $3N$-dimensional configuration space)

$$\Omega = \{\mathbf{R} \in R^{3N} \,|\, U(\mathbf{R}) = U_0\}\,. \tag{1}$$

Geodesic motion on Ω is termed NVU dynamics in analogy with standard Newtonian NVE dynamics, which conserves the total energy E. Motivations for studying NVU dynamics were given in Paper I. The present paper compares NVU dynamics to four other dynamics, two deterministic and two stochastic, concluding that NVU dynamics is a fully valid molecular dynamics.

The path of shortest distance between two points on a Riemannian manifold is a so-called geodesic curve. By definition a geodesic is a curve of stationary length, i.e., one for which small curve variations keeping the two end points $\mathbf{R}_A$ and $\mathbf{R}_B$ fixed, to lowest order do not change the curve length,

$$\delta \int_{\mathbf{R}_A}^{\mathbf{R}_B} dl = 0\,. \tag{2}$$

By discretizing this condition and carrying out the variation, keeping the potential energy fixed by introducing Lagrangian multipliers, the following "basic NVU algorithm" was derived in Paper I ($\mathbf{F}$ is the $3N$-dimensional force vector and i is the time-step index):

$$\mathbf{R}_{i+1} = 2\mathbf{R}_i - \mathbf{R}_{i-1} - 2\,\frac{\mathbf{F}_i \cdot (\mathbf{R}_i - \mathbf{R}_{i-1})}{\mathbf{F}_i^2}\mathbf{F}_i\,. \tag{3}$$

This algorithm works well, but for very long simulations numerical errors accumulate and U drifts to higher values ("entropic drift," see Paper I). This problem is also encountered for the total energy in NVE algorithms,[2] and it is not more severe for NVU than for NVE dynamics. A fully stable NVU algorithm was developed in Paper I, which may be summarized as follows. If one switches to the leap-frog representation and defines the position changes by $\mathbf{\Delta}_{i+1/2} = \mathbf{R}_{i+1} - \mathbf{R}_i$, the stable NVU algorithm is: $\mathbf{\Delta}_{i+1/2} = l_0\,\mathbf{A}_{i+1/2}/|\mathbf{A}_{i+1/2}|$ where l_0 is the step length and $\mathbf{A}_{i+1/2} = \mathbf{\Delta}_{i-1/2} + (-2\mathbf{F}_i \cdot \mathbf{\Delta}_{i-1/2} + U_{i-1} - U_0)\mathbf{F}_i/\mathbf{F}_i^2$. Just as for standard NVE dynamics a final stabilization introduced is to adjust the position changes slightly, e.g., every 100th step, in order to eliminate numerical drift of the center of mass coordinate. In the simulations reported below, we used the fully stable NVU algorithm. However, since the stabilization is merely a technicality, the basic NVU algorithm Eq. (3) is used for theoretical considerations.

Constant-potential-energy algorithms were previously considered in papers dating back to 1986 by Cotterill and Madsen *et al.*[3] and in 2002 by Scala *et al.*[4] In the same spirit, but in a slightly different context, Stratt and co-workers in 2007 and 2010 considered geodesic motion in the space of

a)Electronic mail: dyre@ruc.dk.

points with potential energy less than or equal to U_0.[5] In the thermodynamic limit these points are almost all of potential energy very close to U_0. We refer to Paper I for further discussion of how NVU dynamics relates to these earlier works.

NVU dynamics invites to an alternative view of molecular motion. Instead of focusing on the standard potential-energy landscape in $3N+1$ dimensions,[6] NVU dynamics adopts the configuration-space microcanonical viewpoint and focuses on the $(3N-1)$-dimensional Riemannian hypersurface Ω. The classical potential-energy landscape picture draws attention to the stationary points of the potential-energy function, in particular its minima, the so-called inherent states.[6] In contrast, all points on Ω have the same probability in NVU dynamics and there are no energy barriers – all barriers are of entropic nature defining unlikely parts of Ω that must be passed.[3–5] Despite the absence of energy barriers in the ordinary sense of this term, NVU dynamics is fully able to describe locally activated events (hopping processes between local potential-energy minima). The NVU "heat bath" is provided by the multitude of configurational degrees of freedom.[3–5]

The present paper compares NVU dynamics to other molecular dynamics, including stochastic ones. We first compare to NVE dynamics, which is also deterministic, and conclude that for large systems the two dynamics are basically equivalent. We proceed to compare to other kinds of dynamics, inspired by previous works: The first investigation providing long-time simulations that compared different dynamics (Newtonian versus Langevin) was presented by Gleim *et al.*[7] They studied the Kob-Andersen binary Lennard-Jones (KABLJ) mixture[8] at different temperatures and found that below a certain temperature ($T < 0.8$), the temperature dependence of the diffusion constant and of the structural relaxation time was identical for the two dynamics. This type of investigation was extended by Szamel *et al.*[9] to Brownian dynamics, i.e., stochastic dynamics without the momentum degrees of freedom. They found power-law fitting exponents for the temperature dependence of the diffusion constant and relaxation time very close to those of NVE dynamics. Subsequently, Berthier *et al.*[10] investigated Monte Carlo dynamics for which agreement with Newtonian dynamics was also established, both for a strong and a fragile model glass former (an SiO_2 model and the KABLJ model). This, however, did not apply for higher-order time-correlation functions, a fact contributed to the presence of different conservation laws.[10]

We compare below NVU dynamics to the following four other dynamics: Newtonian dynamics (NVE), Nosé-Hoover NVT dynamics,[11] Monte Carlo dynamics (MC),[12] and a diffusive small-step random-walk dynamics on the constant-potential-energy hypersurface (RW). Section II compares NVU dynamics with the "true" (NVE) time evolution defined by Newton's second law. This is done by simulations of the KABLJ liquid, as well as of the Weeks-Chandler-Andersen (WCA) approximation[13] to the KABLJ liquid (KABWCA) and the Lennard-Jones Gaussian liquid. Section III gives arguments for the equivalence of NVU and NVE dynamics in the thermodynamic limit. Section IV compares NVU dynamics with NVT, MC, and RW dynamics. Section V gives a brief summary and outlook.

II. SIMULATIONS COMPARING *NVU* DYNAMICS TO *NVE* DYNAMICS

In NVU dynamics a geodesic is traced out in configuration space. Physically, this curve may be traversed with any velocity; comparing however to NVE dynamics suggests an obvious time measure for NVU dynamics, as we shall see now. Limiting ourselves for simplicity to systems of particles with identical masses m, the Verlet algorithm for NVE dynamics with time step Δt_{NVE} is[2,14]

$$\mathbf{R}_{i+1} = 2\mathbf{R}_i - \mathbf{R}_{i-1} + \frac{(\Delta t_{NVE})^2}{m}\mathbf{F}_i\,. \tag{4}$$

Comparing to Eq. (3) suggests the following identification of a NVU time step $\Delta t_{i,NVU}$

$$\frac{(\Delta t_{i,NVU})^2}{m} = -2\,\frac{\mathbf{F}_i\cdot(\mathbf{R}_i-\mathbf{R}_{i-1})}{\mathbf{F}_i^2}\,. \tag{5}$$

This quantity is identical to $l_0\lambda_i$ of Paper I. Our simulations show that the average of the right-hand side is always

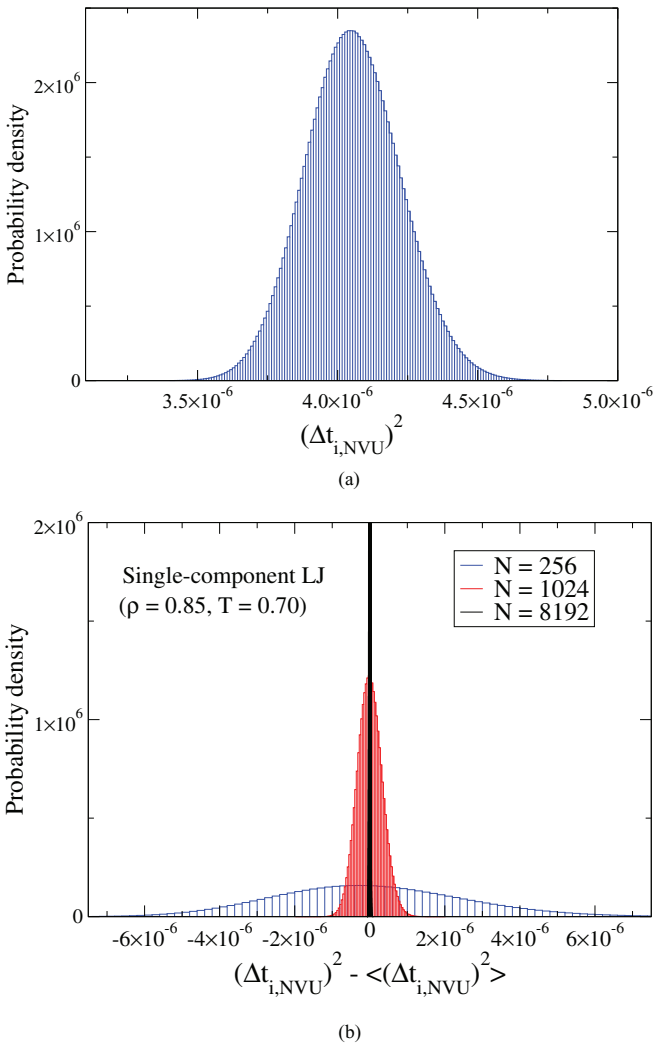

FIG. 1. (a) Probability density of $(\Delta t_{i,NVU})^2$ given by Eq. (5) for the Kob-Andersen binary Lennard-Jones (KABLJ) liquid at $\rho = 1.2$ and $T = 0.44$; (b) Probability density for $(\Delta t_{i,NVU})^2 - \langle(\Delta t_{i,NVU})^2\rangle$ for 256, 1024, and 8192 particles of the single-component LJ liquid ($T = 0.70$, $\rho = 0.85$), showing a narrowing as the particle number increases.

positive for small l_0. We have no proof of this, but presumably it applies rigorously in the thermodynamic limit.

Data are given below in terms of the natural units for the Lennard-Jones pair potential; for the KABLJ and KABWCA system length and energy are given in units of the large-particle parameters σ_{AA} and ϵ_{AA}, respectively. The system sizes are $N = 1024$, 1000, and 1024 for KABLJ, KABWCA, and Lennard-Jones Gaussian, respectively.

The probability distribution of $(\Delta t_{i,NVU})^2$ is given in Fig. 1(a) for an $N = 1024$ KABLJ liquid at $\rho = 1.2$ and $T = 0.44$.[15] The simulations behind this, as well as all below figures, were initiated by choosing the two initial configurations from a well-equilibrated NVE simulation. The target potential energy U_0 in the NVU simulation was chosen as $U_0 = \langle U \rangle_{NVE}$ at the relevant state points. The probability distribution of Fig. 1 is a Gaussian, which is consistent with the fact that $(\Delta t_{i,NVU})^2$ is a sum of many terms that are uncorrelated for large spatial separations.

In view of the above, for comparing NVU and NVE generated sequences we define the NVU time step length Δt_{NVU}

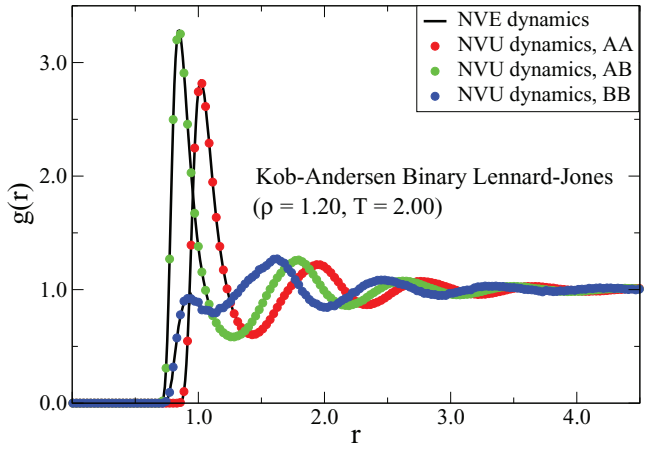

FIG. 2. Radial distribution functions for the KABLJ system at $\rho = 1.2$. The black lines give results from NVE simulations, colored circles from NVU simulation where green, red, and blue denote, respectively, AB, AA, and BB pairs for: (a) $T = 2.0$ and (b) $T = 0.405$.

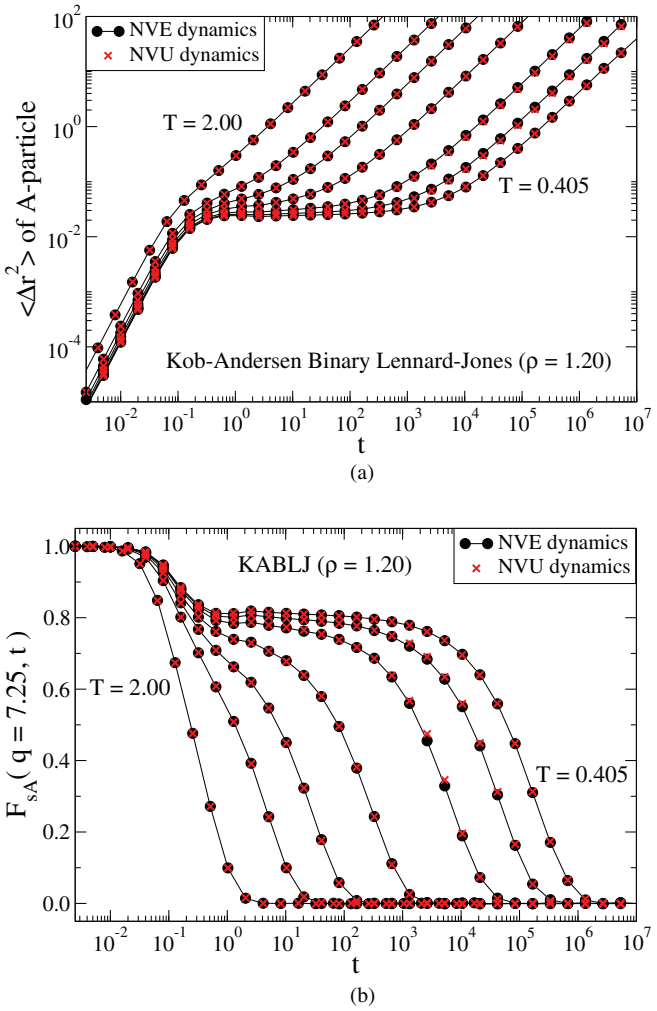

FIG. 3. (a) Mean-square displacement and (b) incoherent intermediate scattering function at the wave vector of the first peak of the AA structure factor. Both simulations were performed at $\rho = 1.2$ for $T = 2.0$, 0.80, 0.60, 0.50, 0.44, 0.42, and 0.405 (left to right) for the KABLJ liquid (1024 particles). NVE dynamics is given by the filled black circles connected by straight lines, NVU dynamics by the red crosses.

as the average of Eq. (5), i.e.,

$$\frac{(\Delta t_{NVU})^2}{m} \equiv -2 \left\langle \frac{\mathbf{F}_i \cdot (\mathbf{R}_i - \mathbf{R}_{i-1})}{\mathbf{F}_i^2} \right\rangle . \tag{6}$$

First, we compare static averages of NVU and NVE simulations. Figure 2 shows the three radial distribution functions for the KABLJ liquid at two different state points. Clearly, the two algorithms give identical results. Next, Fig. 3 shows NVU and NVE results for the mean-square displacement and the incoherent intermediate scattering function of the KABLJ liquid at density $\rho = 1.2$ over a range of temperatures. The mean-square displacement and the incoherent scattering function are both identical for NVU and NVE dynamics.

Corresponding figures are shown in Fig. 4 for the Weeks-Chandler-Andersen (WCA) approximation, which cuts off interactions beyond the energy minima, i.e., keep only the repulsive part of the potential. The WCA version of the system has a similar structure, but a much faster dynamics in the su-

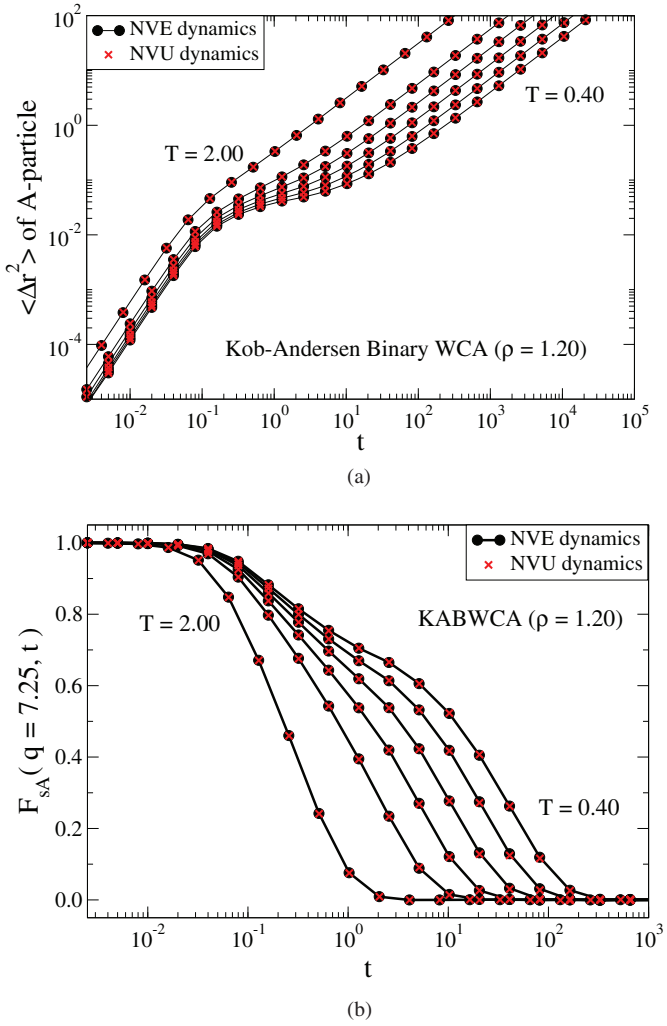

FIG. 4. (a) Mean-square displacement and (b) incoherent intermediate scattering function at the same wave vector as in Fig. 3. Both simulations were performed at $\rho = 1.2$ for $T = 2.0$, 0.80, 0.60, 0.50, 0.44, and 0.40 (left to right) for the WCA approximation to the KABLJ liquid. NVE dynamics is given by the filled black circles connected by straight lines, NVU dynamics by the red crosses.

percooled regime.[16,17] Again, NVU and NVE dynamics give identical results.

We also studied the so-called Lennard-Jones Gaussian system defined by a pair potential that adds a Gaussian to a LJ potential,[18] a liquid that is not strongly correlating.[16] Figure 5 shows that for this model the incoherent intermediate scattering function is also the same for NVU and NVE dynamics. In summary, for all systems simulated, we found $NVU = NVE$. This applies even for $N = 65$ particles of the KABLJ liquid ($T = 0.8$, $\rho = 1.2$).

III. ARGUMENTS FOR THE EQUIVALENCE OF *NVU* AND *NVE* DYNAMICS AS $N \to \infty$

The above results raise the question: Are NVU and NVE dynamics mathematically equivalent in some well-defined sense? The two algorithms are not identical, of course; that would require no variation in the quantity $\Delta t_{i,NVU}$ (Fig. 1). On the other hand, the $\Delta t_{i,NVU}$

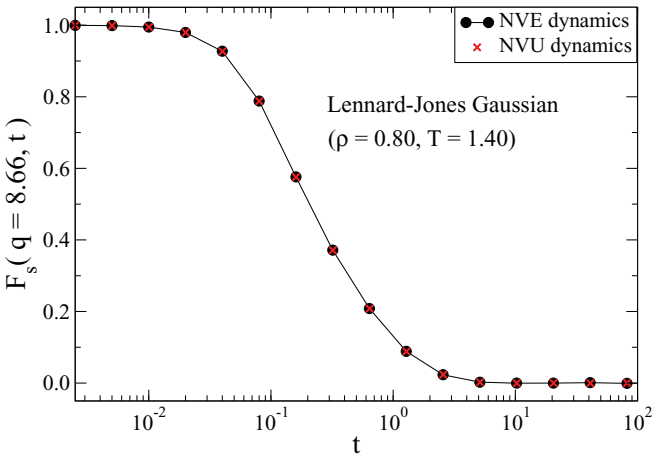

FIG. 5. The incoherent intermediate scattering function at $\rho = 0.8$ and $T = 1.4$ for the Lennard-Jones Gaussian system.[18] The black circles represent a NVE simulation, the red symbols represent a NVU simulation.

distribution narrows as the particle number increases [Fig. 1 (b)]. From this NVU and NVE dynamics are expected to become equivalent for $N \to \infty$ in the following sense: For any configurational quantity A with zero average, to leading order in $1/N$ there is identity of dynamic quantities such as the time-autocorrelation function $\langle A(0)A(t)\rangle$ or the mean-square change $\langle \Delta^2 A(t)\rangle$ (i.e., the relative deviations go to zero as $N \to \infty$). Consider the time-autocorrelation function of an extensive quantity A with zero average. In this case, the time-autocorrelation function scales in both ensembles as N, and the proposed equivalence of the dynamics means that $|\langle A(0)A(t)\rangle_{NVU} - \langle A(0)A(t)\rangle_{NVE}| \propto N^0$ as $N \to \infty$. Intuitively, what happens is that since in NVE dynamics the relative potential-energy fluctuations go to zero as $N \to \infty$, it becomes a better and better approximation to regard the potential energy as conserved.[5]

There exists in analytical mechanics a variational principle that does not involve time. This is the Maupertuis principle from 1746,[20,21] a variational principle that is originally due to Jacobi and for this reason is sometimes referred to as "Jacobi's form of the least action principle."[19,21] This states that a classical-mechanical system of fixed energy E follows a curve in configuration space obeying (with fixed end points)

$$\delta \int_{\mathbf{R}_A}^{\mathbf{R}_B} \sqrt{2m(E-U)}\, dl \;=\; 0\,. \tag{7}$$

One may argue that the relative variations of the integrand go to zero as $N \to \infty$. Thus, the integrand in this limit becomes effectively constant and can be taken outside the variation, implying Eq. (2) for motion which in the same limit effectively takes place on the constant-potential-energy hypersurface.[5]

If l is the path length parametrizing the path, Eq. (7) implies[19,20] $d^2\mathbf{R}/dl^2 = [\mathbf{F} - (\mathbf{F}\cdot\mathbf{t})\mathbf{t}]/2(E - U(\mathbf{R}))$ where $\mathbf{t} = d\mathbf{R}/dl$ is the unit vector tangential to the path. The term $\mathbf{F} - (\mathbf{F}\cdot\mathbf{t})\mathbf{t}$ is the (vector) component of the force normal to the path. In the thermodynamic limit the path as mentioned approaches more and more the constant-potential-energy hypersurface Ω, i.e., $\mathbf{F}\cdot\mathbf{t} = 0$. In this limit, one has also $dl \propto dt$ because the relative kinetic energy fluctuations go to

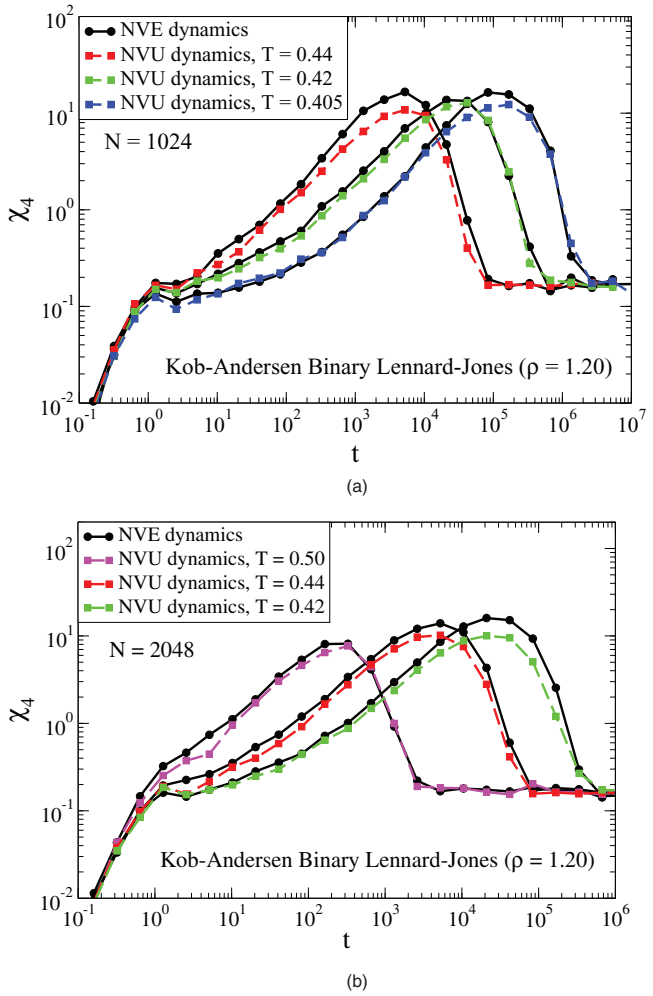

FIG. 6. (a) The dynamical fluctuations quantified by $\chi_4(t)$ for the A particles at $\rho = 1.2$ for a KABLJ liquid with 1024 particles. The black circles give results for an NVE simulation, the red, green, and blue symbols represent NVU simulations at, respectively, $T = 0.44$, 0.42, 0.405. (b) The dynamical fluctuations quantified by $\chi_4(t)$ for the A particles at $\rho = 1.2$ for the KABLJ system with 2048 particles. The black circles give results for a NVE simulation, the violet, red, and green symbols represent NVU simulations of, respectively, $T = 0.50$, 0.44, and 0.42. Increasing the number of particles does not appear to decrease the deviation between the two dynamics.

zero. In this way, in the thermodynamic limit the Maupertuis principle is equivalent to both the geodesic equation Eq. (2) and to Newton's second law $\ddot{\mathbf{R}} = \mathbf{F}/m$.

The equivalence of NVU and NVE dynamics in the thermodynamic limit relates to static averages as well as to time-autocorrelation functions of extensive quantities with zero average. Just as one must be careful when comparing fluctuations between different ensembles, fluctuations relating to the dynamics need not be the same for NVU and NVE dynamics. As an example, Fig. 6 shows the quantity $\chi_4(t)$ defined by $\chi_4(t) = N_A\,[\,\langle F_{sA}^2(\mathbf{k},t)\rangle - \langle F_{sA}(\mathbf{k},t)\rangle^2\,]$ for the KABLJ system at three temperatures and two values of N. χ_4 quantifies the incoherent intermediate scattering function fluctuations.[22] For $\chi_4(t)$, NVU and NVE dynamics do not appear to give identical results. A related observation was made by Berthier *et al.*, who showed that $\chi_4(t)$ is not the same in NVE and NVT dynamics.[10]

IV. COMPARING *NVU* DYNAMICS TO *NVT*, MONTE CARLO, AND DIFFUSIVE DYNAMICS ON Ω

This section compares simulations using NVU dynamics to results for three other dynamics, two of which are standard. We focus on the viscous regime. One dynamics is the Nosé-Hoover NVT dynamics, a deterministic sampling of the NVT canonical ensemble that may be derived from a "virtual" Hamiltonian.[11,23] The second standard dynamics considered is the Metropolis Monte Carlo (MC) algorithm, which generates a stochastic sequence of states giving the correct NVT canonical ensemble distribution. The third dynamics employed below is also stochastic; it simulates diffusion on the constant-potential-energy hypersurface Ω by a small step-length random walk (RW) on Ω. This was discussed by Scala *et al.*,[4] who proposed the following equation of motion:

$$\frac{d\mathbf{R}_i}{dt} = \Delta\boldsymbol{\eta}_i - \frac{\Delta\boldsymbol{\eta}_i \cdot \mathbf{F}_i}{\mathbf{F}_i^2}\mathbf{F}_i\,, \tag{8}$$

where $\Delta\boldsymbol{\eta}_i$ is a $3N$-dimensional random vector (see below). Equation (8) implies $\mathbf{F}_i \cdot \dot{\mathbf{R}}_i = 0$, which ensures the potential-energy conservation required for staying on Ω.

The RW algorithm was discretized and implemented as a "predictor-corrector" algorithm in the following way. A vector $\Delta\boldsymbol{\eta}_i$ was chosen from a cube with length $L = 0.01\sigma$. This is small enough to ensure that the dynamics generates the correct NVE radial distribution function and at the same time has no effect on the average dynamical quantities. Positions were updated via

$$\mathbf{R}_{i+1} = \mathbf{R}_i + \Delta t\,\Delta\boldsymbol{\eta}_i - \frac{\Delta t\,\Delta\boldsymbol{\eta}_i \cdot \mathbf{F}_i}{\mathbf{F}_i^2}\mathbf{F}_i\,. \tag{9}$$

Finally, $\mathbf{R}_{i+1}$ was corrected by applying two iterations of $\mathbf{R}_{i+1} \equiv \mathbf{R}_{i+1} - \frac{U_{i+1}-U_0}{\mathbf{F}_{i+1}^2}\mathbf{F}_{i+1}$ in order to eliminate long-time entropic drift of the potential energy.

MC and RW dynamics involve no generic measures of time. We compared their results to NVU dynamics by proceeding as follows. At any given state point the time-scaling factor was determined from the long-time behavior

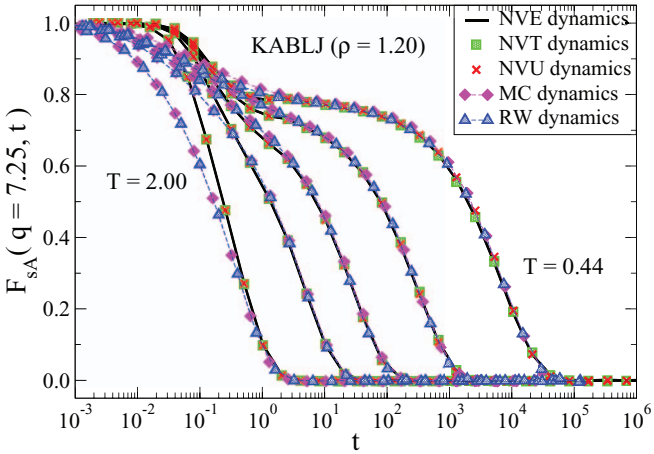

FIG. 7. The incoherent intermediate scattering function for all five investigated dynamics for the KABLJ liquid at $\rho = 1.2$ and $T = 2.0$, 0.80, 0.60, 0.50, and 0.44. The black curve is the NVE simulation, red crosses: NVU, green squares: NVT, magenta diamonds: MC, blue triangles: RW.

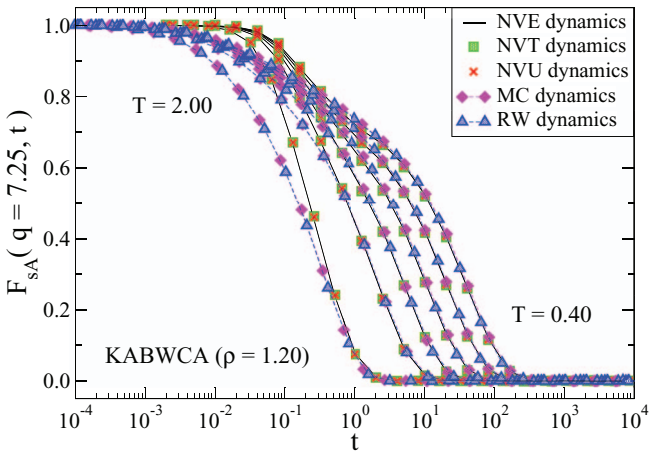

FIG. 8. The incoherent intermediate scattering function for all five investigated dynamics for the KABWCA system at $\rho = 1.2$ and $T = 2.0$, 0.80, 0.60, 0.50, 0.44, and 0.40. The black curve is the NVE simulation, red crosses: NVU, green squares: NVT, magenta diamonds: MC, blue triangles: RW.

of the mean-square displacement by requiring that the single-particle displacement obeys $\langle \Delta x^2(t) \rangle = 2Dt$ for $t \to \infty$ with the NVE diffusion constant D. By construction, this ensures agreement with the long-time mean-square displacement of NVE dynamics.

In Fig. 7, we show the incoherent intermediate scattering function of the KABLJ liquid for all investigated dynamics at several state points. A corresponding figure for the KABWCA system is shown in Fig. 8.

NVU and NVT dynamics agree quantitatively for all investigated state points. This is not surprising given the results of Secs. II and III and the well-known fact that NVE and NVT dynamics give the same time-autocorrelation functions to leading order in $1/N$.[24] The incoherent intermediate scattering functions of MC and RW agree at all investigated temperatures. This is consistent with the recent results of Berthier *et al.*,[10] who compared Langevin to MC dynamics. For lower temperatures ($T < 0.80$) quantitative agreement is found among all five dynamics investigated in the α-relaxation regime.

V. SUMMARY AND OUTLOOK

NVU dynamics traces out geodesic curves on the $(3N-1)$-dimensional potential-energy hypersurface Ω. We have compared NVU dynamics with four other dynamics. Simulations supplemented by non-rigorous analytical arguments showed that NVU and NVE dynamics are equivalent in the thermodynamic limit, i.e., typical autocorrelation functions become identical to leading order in $1/N$. Furthermore, NVU dynamics was compared to two stochastic dynamics, standard Monte Carlo dynamics and a small-step random walk on the constant-potential-energy hypersurface Ω representing diffusion on Ω. Agreement was established for all dynamics, including also NVT dynamics, in the α-relaxation regime where inertial effects are unimportant. We conclude that NVU dynamics is a fully valid molecular dynamics.

It is interesting to note that NVU dynamics, like any geodesic motion on a Riemannian manifold, can be formulated as a Hamiltonian dynamics based on the curved-space purely kinetic energy Hamiltonian $H = 1/2 \sum_{a,b} g_{ab}(x) p^a p^b$ where x is the manifold coordinate, g_{ab} is the corresponding metric tensor, and p_a are the generalized momenta.[25] Indeed, long ago Hertz argued that one should focus exclusively on the kinetic energy and describe classical mechanics as a geodesic motion on a high-dimensional Riemannian manifold (along the "geradeste Bahn" of this manifold, the straightest curve).[26] Hertz' idea was to eliminate the force and potential energy concepts entirely from mechanics and replace particle interactions by constraints among the coordinates; the relevant manifold is defined by these constraints. This is not what we have done here. There is nevertheless the fundamental similarity between the Hertz and the NVU approaches that both are built on the conceptual simplification of "replacing Newton's second law by Newton's first law." Moreover, as shown in the Appendix, the effect of masses enters into the metric of the Riemannian manifold in precisely the same way as we need for NVU dynamics when this is generalized to deal with systems of varying masses. Thus, NVU dynamics realizes Hertz's ideas to a large extent.

From a technical point of view NVU dynamics offers few advantages because it is not faster than NVE or NVT dynamics. However, by referring directly to the properties of a Riemannian differentiable manifold, NVU dynamics leads to an alternative way of thinking about the classical mechanics of many-particle systems. Future work should focus on relating the mathematical properties of Ω to the physical properties of the system in question. It is our hope that in this way new insights into liquid dynamics may be arrived at by adopting the NVU viewpoint.

ACKNOWLEDGMENTS

Useful inputs from Ole J. Heilmann and Nick Bailey are gratefully acknowledged. The centre for viscous liquid dynamics "Glass and Time" is sponsored by the Danish National Research Foundation (DNRF).

APPENDIX: GENERALIZATION OF THE *NVU* ALGORITHM TO DEAL WITH SYSTEMS OF DIFFERENT PARTICLE MASSES

Papers I and II deal with systems of particles with identical mass m. The basic NVU algorithm Eq. (3), however, is well defined and works perfectly well for any classical mechanical system. The algorithm traces out a geodesic on Ω that is independent of the particles' masses, a geometrical path entirely determined from the function $U(\mathbf{r}_1, \ldots, \mathbf{r}_N)$. Equation (5), which ensures $NVU = NVE$ in the thermodynamic limit, only works if all particles have mass m. On the other hand, the question arises if a generalization of Eq. (3) is possible ensuring that $NVU = NVE$ as $N \to \infty$ also for systems of particles with different masses.

If the kth particle mass is m_k, we seek to modify the basic NVU algorithm such that it, for the kth particle as $N \to \infty$, converges to (where $\mathbf{r}^{(k)}$ is the coordinate of the kth particle,

$\mathbf{F}^{(k)}$ is the force on it, and the subscript j is the time step index)

$$\mathbf{r}_{j+1}^{(k)} = 2\,\mathbf{r}_j^{(k)} - \mathbf{r}_{j-1}^{(k)} + \frac{(\Delta t)^2}{m_k}\mathbf{F}_j^{(k)}\,. \tag{A1}$$

If the average mass is denoted by $\langle m\rangle$, we define reduced masses by

$$\tilde{m}_k \equiv \frac{m_k}{\langle m\rangle}\,. \tag{A2}$$

A geodesic is defined by giving the shortest distance between any two of its close-by points. In Paper I and in Eq. (2) of the present paper the distance measure is given by the standard Euclidian distance $dl^2 = \sum_k d\mathbf{r}^{(k)} \cdot d\mathbf{r}^{(k)}$. A change of metric leads to different geodesics. Consider the following metric:

$$dl^2 = \sum_k \tilde{m}_k\, d\mathbf{r}^{(k)} \cdot d\mathbf{r}^{(k)}. \tag{A3}$$

This is precisely the metric discussed by Hertz in his mechanics long ago.[26] In the "Hertzian" metric the discretized path length used in deriving the NVU algorithm is (Paper I) $\sum_j \sqrt{\sum_k \tilde{m}_k(\mathbf{r}_j^{(k)} - \mathbf{r}_{j-1}^{(k)})^2}$ (j is the time step index). Thus, the variational condition becomes

$$\delta\left(\sum_j \sqrt{\sum_k \tilde{m}_k\left(\mathbf{r}_j^{(k)} - \mathbf{r}_{j-1}^{(k)}\right)^2} - \sum_j \lambda_j U(\mathbf{R}_j)\right) = 0\,. \tag{A4}$$

From this it follows via the *ansatz* of constant step length that

$$\mathbf{r}_{j+1}^{(k)} = 2\mathbf{r}_j^{(k)} - \mathbf{r}_{j-1}^{(k)} - \frac{2[\mathbf{F}_j \cdot (\mathbf{R}_j - \mathbf{R}_{j-1})]\mathbf{F}_j^{(k)}}{\tilde{m}_k \mathbf{F}_j^2}. \tag{A5}$$

This translates into Eq. (A1) for a suitably chosen Δt; likewise, the relative fluctuations of the term $2[\mathbf{F}_j \cdot (\mathbf{R}_j - \mathbf{R}_{j-1})]/\mathbf{F}_j^2$ go to zero in the thermodynamic limit ($N \to \infty$) such that $NVU = NVE$ in this limit.

[1] T. S. Ingebrigtsen, S. Toxvaerd, O. J. Heilmann, T. B. Schrøder, and J. C. Dyre, J. Chem. Phys. **135**, 104101 (2011).

[2] M. P. Allen and D. J. Tildesley, *Computer Simulation of Liquids* (Oxford Science, Oxford, 1987); D. Frenkel and B. Smit, *Understanding Molecular Simulation* (Academic, New York, 2002).

[3] R. M. J. Cotterill, Phys. Rev. B **33**, 262 (1986); R. M. J. Cotterill and J. U. Madsen, in *Characterizing Complex Systems*, edited by H. Bohr (World Scientific, Singapore, 1990), p. 177; J. Li, E. Platt, B. Waszkowycz, R. Cotterill, and B. Robson, Biophys. Chem. **43**, 221 (1992); R. M. J. Cotterill and J. U. Madsen, J. Phys.: Condens. Matter **18**, 6507 (2006).

[4] A. Scala, L. Angelani, R. Di Leonardo, G. Ruocco, and F. Sciortino, Philos. Mag. B **82**, 151 (2002).

[5] C. Wang and R. M. Stratt, J. Chem. Phys. **127**, 224503 (2007); C. Wang and R. M. Stratt, **127**, 224504 (2007); C. N. Nguyen and R. M. Stratt, J. Chem. Phys. **133**, 124503 (2010).

[6] M. Goldstein, J. Chem. Phys. **51**, 3728 (1969); F. H. Stillinger, Science **267**, 1935 (1995); F. Sciortino, J. Stat. Mech.: Theory Exp. **2005**, 35 (2005); A. Heuer, J. Phys.: Condens. Matter **20**, 373101 (2008).

[7] T. Gleim, W. Kob, and K. Binder, Phys. Rev. Lett. **81**, 4404 (1998).

[8] W. Kob and H. C. Andersen, Phys. Rev. E **51**, 4626 (1995); **52**, 4134 (1995).

[9] G. Szamel and E. Flenner, Europhys. Lett. **67**, 779 (2004); E. Flenner and G. Szamel, Phys. Rev. E **72**, 011205 (2005).

[10] L. Berthier and W. Kob, J. Phys.: Condens. Matter **19**, 205130 (2007); L. Berthier, Phys. Rev. E **76**, 011507 (2007).

[11] S. Nosé, J. Chem. Phys. **81**, 511 (1984); W. G. Hoover, Phys. Rev. A **31**, 1695 (1985).

[12] N. Metropolis, A. W. Rosenbluth, M. N. Rosenbluth, A. H. Teller, and E. Teller, J. Chem. Phys. **21**, 1087 (1953).

[13] J. D. Weeks, D. Chandler, and H. C. Andersen, J. Chem. Phys. **54**, 5237 (1971).

[14] L. Verlet, Phys. Rev. **159**, 98 (1967).

[15] All simulations were performed using a molecular dynamics code optimized for NVIDIA graphics cards, which is available as open source code at http://rumd.org.

[16] U. R. Pedersen, N. P. Bailey, T. B. Schrøder, and J. C. Dyre, Phys. Rev. Lett. **100**, 015701 (2008); U. R. Pedersen, T. Christensen, T. B. Schrøder, and J. C. Dyre, Phys. Rev. E **77**, 011201 (2008); T. B. Schrøder, U. R. Pedersen, N. P. Bailey, S. Toxvaerd, and J. C. Dyre, Phys. Rev. E **80**, 041502 (2009); N. P. Bailey, U. R. Pedersen, N. Gnan, T. B. Schrøder, and J. C. Dyre, J. Chem. Phys. **129**, 184507 (2008); N. P. Bailey, U. R. Pedersen, N. Gnan, T. B. Schrøder, and J. C. Dyre, J. Chem. Phys. **129**, 184508 (2008); T. B. Schrøder, N. P. Bailey, U. R. Pedersen, N. Gnan, and J. C. Dyre, J. Chem. Phys. **131**, 234503 (2009); N. Gnan, T. B. Schrøder, U. R. Pedersen, N. P. Bailey, and J. C. Dyre, J. Chem. Phys. **131**, 234504 (2009); N. Gnan, C. Maggi, T. B. Schrøder, and J. C. Dyre, Phys. Rev. Lett. **104**, 125902 (2010); T. B. Schrøder, N. Gnan, U. R. Pedersen, N. P. Bailey, and J. C. Dyre, J. Chem. Phys. **134**, 164505 (2011).

[17] U. R. Pedersen, T. B. Schrøder, and J. C. Dyre, Phys. Rev. Lett. **105**, 157801 (2010).

[18] V. V. Hoang and T. Odagaki, Physica B **403**, 3910 (2008). The Lennard-Jones Gaussian pair potential is $\varepsilon\left[(\sigma/r)^{12} - 2(\sigma/r)^6 - \varepsilon_0 \exp((r-r_0)^2/2\sigma_0^2)\right]$ where $\sigma_0 = 0.14$, $\varepsilon_0 = 1.5$, and $r_0 = 1.47$.

[19] E. T. Whittaker, *A Treatise on the Analytical Dynamics of Particles and Rigid Bodies*, 4th ed. (Cambridge University Press, Cambridge, England, 1999); H. Goldstein, *Classical Mechanics* (Addison-Wesley, Reading, MA, 1950).

[20] L. D. Landau and E. M. Lifshitz, *Mechanics*, 2nd ed. (Pergamon, Oxford, 1969).

[21] Wikipedia article "Maupertuis' principle," see http://wikipedia.org.

[22] C. Toninelli, M. Wyart, L. Berthier, G. Biroli, and J.-P. Bouchaud, Phys. Rev. E **71**, 041505 (2005).

[23] S. Toxvaerd, Mol. Phys. **72**, 159 (1991); T. Ingebrigtsen, O. J. Heilmann, S. Toxvaerd, and J. C. Dyre, J. Chem. Phys. **132**, 154106 (2010).

[24] D. J. Evans and B. L. Holian, J. Chem. Phys. **83**, 4069 (1985).

[25] Wikipedia article "Geodesics as Hamiltonian flows," see http://wikipedia.org.

[26] H. Hertz, *Die Prinzipien der Mechanik, in Neuem Zusammenhange Dargestellt* (Johann Ambrosius Barth, Leipzig, 1894); J. Lützen, Arch. Hist. Exact Sci. **49**, 1 (1995); J. Lützen, *Mechanistic Images in Geometric Form: Heinrich Hertz's "Principles of Mechanics"* (Oxford University Press, Oxford, 2005); J. Preston, Stud. Hist. Philos. Sci. **39**, 91 (2008).